Доклади на Българската академия на науките
Comptes rendus de l'Académie bulgare des Sciences
Tome 76, No 10, 2023

ENGINEERING SCIENCES

Renewable energy

ANALYSIS OF AWPI BASED HYBRID GRID-TIED INVERTER FOR SMART ENERGY MANAGEMENT SYSTEM

Sheikameer Batcha[#], Sudha Mohanram[*]

Received on March 23, 2023
Presented by P. Petkov, Corresponding Member of BAS, on June 27, 2023

Abstract

Renewable energy sources are gaining popularity in recent years for power generation. The world has an abundance of pollution-free solar and wind energy; batteries play vital role for energy storage and all these sources combine to form a hybrid power system. Efficient management of the hybrid system via controlling the operation of its components is essential. In this article, a smart energy management system is proposed, where the control is focused on the hybrid grid-tied inverter. The inverter module is controlled through an anti-windup proportional-integral (AWPI) current and voltage controller. The performance of the proposed control system has been analyzed through current, and voltage Total Harmonic Distortion (THD) before and after grid integration. The suggested AWPI controller effectively mitigated the voltage drop and maintained the THD within the appropriate level. In addition, the proposed scheme of interest enhanced the steady-state response of the smart-grid system. The comparative analysis made among the intended controller and its counterparts inferred its superiority.

Key words: PV, WECS, microgrid, anti-windup PI controller, smart energy management system

Introduction. Integrating renewable energy sources [1,2] can be used both practically and profitably based on available natural resources. In order to enhance the existing grid's performance with sustainable resources, small-scale power

[#]Corresponding author.
DOI:10.7546/CRABS.2023.10.13

generation is receiving a lot of attention [3–6]. The wind-solar hybrid system can produce power to supply both AC loads with grid integration and DC loads with energy storage [7,8].

The WECS requires a governor capable of ensuring a wind turbine's activity mode around the ideal operating point in order to obtain the most energy possible out of it while the wind speed is changeable. The most frequent and extensively researched approach is MPPT based on tip speed ratio (TSR). In this article, a wind energy conversion system uses a TSR-based MPPT. PV systems must run at maximum power point to capture the massive volume of solar energy [9]. The target operating point is determined using the incremental conductance (InC) approach using source voltage and current information.

Grid-connected inverters play a crucial role in the renewable energy systems, because they facilitate effective power transfer between utility grid and renewable energy sources [10]. To reduce the current harmonics L or LCL filter is used [11–15].

This article aims to present a hybrid energy voltage regulation and to construct a reliable proportional-integral (PI) controller for controlling the grid current while assuming the voltage is constant. In this study, an anti-windup PI controller is used in inverter control to address the windup issue and enhance the performance of grid-tied inverters. A smart energy management System (SEMS) is applied to maintain the power balance in the microgrid and to provide configurable and adaptable control for various scenarios of load demand fluctuations and variations in renewable energy sources [16].

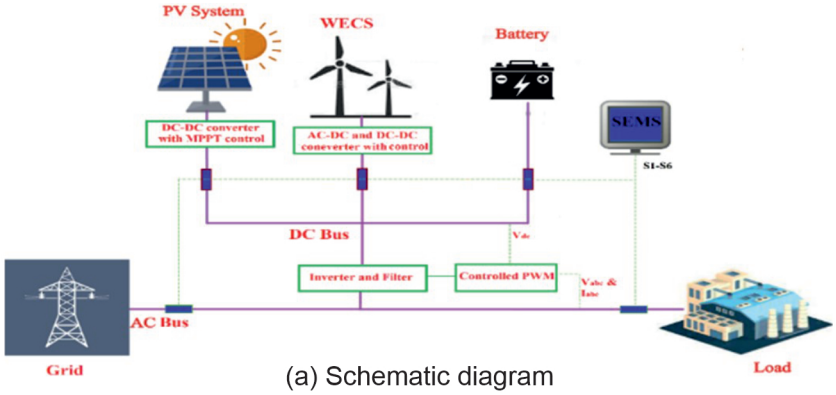
Materials and method. ***Proposed hybrid renewable power system.*** In this article, a standard DC link is applied to organize the DC output of the batteries, solar PV plant, and wind power as depicted in Fig. 1(a). This DC electricity is converted into AC power by means of a conventional inverter. All the Power system, battery charging and discharging, grid integration, and load are managed by a SEMS by relay control of R1–R6, as depicted in Fig. 1(b).

Figure 1(c) is the first order transfer function model of the proposed system, where K_{solar}, K_{wind}, K_{battery}, K_{B1}, K_{b2}, K_{b3}, K_{bu} are the gains and T_{solar}, T_{wind}, T_{battery}, T_{B1}, T_{b2}, T_{b3}, T_{bu} are the time constants of the solar, wind, battery energy Power systems and their converters, respectively. The values of the gain and time constant are substituted in the transfer function as shown in Fig. 1(c) [17].

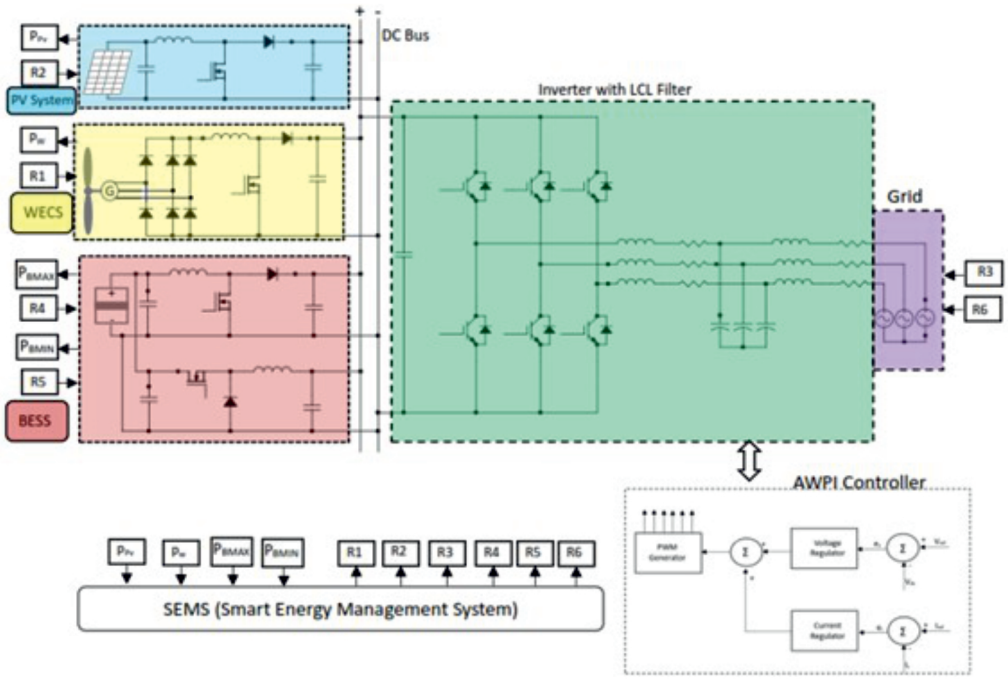
PV power system. PV power system is connected to DC bus via boost converter, while the switching of the boost converter is decided by InC algorithm. The mathematical expression for the output current (I_{pv}) of the solar cell is:

$$I_{pv} = I_{ph} - \Gamma_{ao} \times \left[\exp\left(\frac{(v_{PV} + \phi_{sh} I_{pv}) \times Q}{\eta_{cs} t \delta_c \mu_{fd}}\right) - 1\right] - \frac{v_{pv} + \phi_{sh} I_{pv}}{\varphi_p}, \tag{1}$$

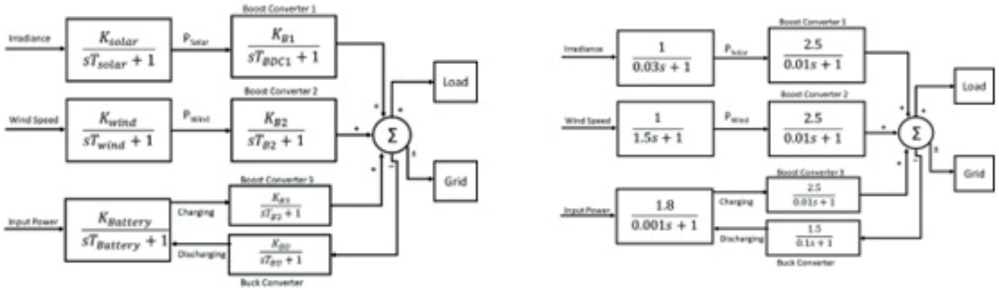
where I_{ph} is the solar current, Γ_{ao} is the leakage current of diode, v_{PV} is the output voltage of cell, ϕ_s and φ_p are the series and parallel resistances, η_{cs} is the



(a) Schematic diagram



(b) Circuit diagram



(c) First order transfer function model

Fig. 1. SEMS with AWPI controller

cells in series, Q is the charge (of an electron), the Boltzmann constant is t, δ_c is a cell temperature, μ_{fd} is ideality factor of the diode.

Wind power system. A wind turbine, a permanent magnet synchronous generator (PMSG), a DC-DC boost converter, and a controller make up the WECS. The following are the techniques through which wind energy is extracted:

$$P_w = \frac{1}{2}\rho A v^3 C_p(\lambda, \theta), \tag{2}$$

$$\lambda = \omega_m R/v, \tag{3}$$

where ρ is the air density in kg/m^3, A is the area swept by the rotor blades in m^2, and v is the wind velocity in m/s. The power coefficient C_p is a function of tip speed ratio (λ) and pitch angle (θ). In equation (3) R is the blade length (in m) and ω_m is the rotor speed (in rad/s). This setup employs a wind turbine with a changeable rotational speed [18].

Battery energy storage system. In this study, a 3 kW battery storage system is investigated. Since rating of DC bus is 680 V, BESS is associated with a buck converter for charging and a boost converter for discharging. Every converter is separately regulated by SEMS. SEMS protects battery from overcharging by restricting $P_{\text{BAT MAX}}$ and prevents battery discharge by restraining $P_{\text{BAT MIN}}$, which are determined depending upon state of charge (SOC) of battery. SOC of battery is defined as

$$\text{SOC} = \frac{Q(t)}{Q_{\text{nom}}}. \tag{4}$$

Inverter with filter. The PV, wind, and battery systems are linked to the DC bus. The DC bus is accompanying to the load and the grid through an inverter. In this investigation, three-phase Hex bridge voltage source inverter is constructed using IGBT. Between the inverter and the grid, a three-phase LCL filter is attached for its effective performance and straightforward modelling.

Inverter control. *PI controller-based inverter control.* In this study, a PI controller is proposed to manage the output voltage by controlling the switching of an inverter. DC link Voltage error (e) is fed to the PI controller to generate reference current (I_d^*) for PWM generation. Grid voltage and current are converted in dq frame. Grid I_d current is compared with I_d^* in a current regulator. Current regulator is also a PI controller results V_d^*. This voltage in dq frame is converted in abc with the angular frequency reference from grid, where V_{abc} acts as reference signal for PMW generator to control inverter. The following equation describes PI controller for inverter:

$$I_d^* = K_p e(t) + \frac{K_i}{s} e(t), \quad e = V_{\text{dc}}^* - V_{\text{dc}}, \tag{5}$$

where K_p is proportional gain, K_i is the integral gain and they are tuned using Ziegler–Nichols method. The integral gain is initially set to zero in this procedure,

and the proportional gain is subsequently increased until the system becomes unstable. The value of K_p at the point of instability is called K_u; the time of settling is T_u, which is used to find the gains K_p and K_i. In this analysis PI controller is designed with $K_p = 7$, $K_i = 400$ for voltage controller, while $K_p = 0.3$, $K_i = 20$ for current controller.

AWPI controller-based inverter control. An integral action in a PI controller frequently creates a rollover or windup issue [19, 20]. This problem happens when the controller's input error is substantial and non-zero for a long time. Consequently, it is necessary to overcome the windup phenomenon using the AWPI approach. Figure 2 depicts the proposed AWPI controller for inverter voltage control.

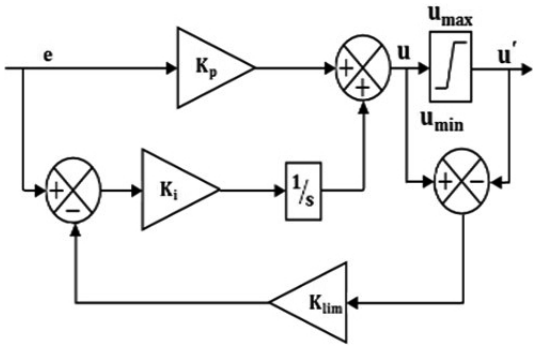


Fig. 2. Simulation model – AWPI controller

Output 'd' can be expressed as

$$I_d^*(t) = \left(X_0 - \frac{e}{K_{\text{lim}}} - I_{\text{dmax}} + K_p \times e\right) \exp(-K_i K_{\text{lim}} t) + \left(\frac{e}{K_{\text{lim}}} + I_{\text{dmax}}\right). \tag{6}$$

Here X_0 is the initial value of state 'x'. If steady state value of 'd' is $\mathrm{d_{ss}}$, then I_{dss} is as follows

$$I_{\text{dss}} = I_{\text{dmax}} + \frac{e}{K_{\text{lim}}}. \tag{7}$$

The steady state and dynamic relationships reveal that while the error input 'e' is negative, the K_{lim} value must be large; so, $I_{\text{dss}} \approx I_{\text{d}}$ and the controller will rapidly shift out of saturation.

For example, assume error is -0.5 V, in this analysis K_{lim} is designed as 100, applying these values in equation (7) gives

$$I_{\text{dss}} = I_{\text{dmax}} + 0.005.$$

In the above calculation e/K_{lim} becomes negligible and the controller comes out of saturation quickly. In an AWPI controller K_p and K_i are designed using

Ziegler–Nichols method similar in a PI controller. In order for the controller to come out of saturation quickly K_{lim} is designed with high value, in this analysis $K_p = 7$, $K_i = 400$ and $K_{\text{lim}} = 100$ for voltage controller, while $K_p = 0.3$, $K_i = 20$ and $K_{\text{lim}} = 100$ for current controller.

Smart energy management system. SEMS constantly monitors power demand, renewable energy sources, and battery status. Using SEMS, the power system operates in several modes dependent on load demand and the availability of sources. The various modes are:

Case 1: If P_{PV} is greater than minimum PV power, then R2=1, otherwise R2=0.

Case 2: If P_w is greater than minimum wind power, then R1=1, otherwise R1=0.

Case 3: If sum of renewable energy is greater than load demand, battery power is less than $P_{\text{bat-max}}$, then battery charging is activated, R5=1.

Case 4: If sum of renewable energy is lesser than load demand, battery power is greater than $P_{\text{bat-min}}$, then battery discharging is activated, R4=1.

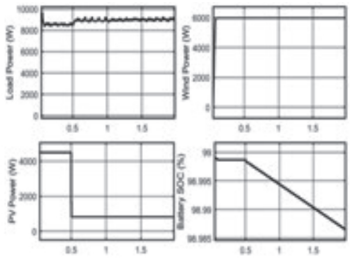
Case 5: If sum of renewable energy is greater than load demand, battery power is greater than $P_{\text{bat-max}}$, power to grid is activated, R6=1.

Case 6: If sum of renewable energy is lesser than load demand, battery power is lesser than or equal to $P_{\text{bat-min}}$, power from grid is activated, R3=1.

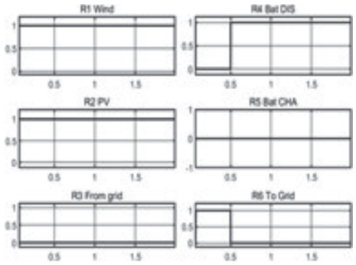
Simulation results and discussion. A simulation model of grid tied renewable power system with SEMS is analyzed using MATLAB/Simulink R2018b. Specifications of the proposed system are PV – 4.5 kW, WECS – 6 kW and BESS – 3 kW. In 0.5 s, the load power is adjusted from 8.5 kW to 9 kW. In this case the PV power is enormous around 4500 W, then it is reduced to 800 W at 0.5 s. Wind power is sustained at 6 kW throughout the duration of operation. The average condition of the battery at startup is 99%. These power statuses and switching conditions controlled by SEMS are shown in Fig. 3.

Figure 3(a) shows that renewable power surpasses load and the battery is charged for 0.5 s. Consequently, surplus energy should be sent to the grid. After 0.5 s, the load power increases while the PV power decreases to 800 W. The battery must be depleted to power the load. Figure 3(b) shows that R1 and R2 are immediately activated due to the availability of PV and wind power. R3 is turned off since the load can be satisfied by available power sources and grid power is not required. Since the battery is fully charged, R5 for battery charging remains off. R6 is activated for 0.5 s to send extra power to the grid. At 0.5 s, the battery is discharged by turning on R4 in order to match the load demand. To analyze the performance of open loop inverter grid integration is activated at 1 s.

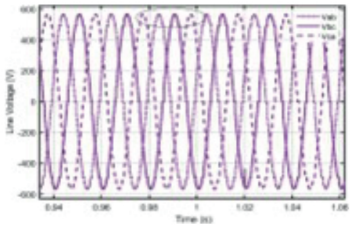
Figure 3(c) shows that the voltage drops by about 4.5 V when an inverter is integrated into the grid. PI and AWPI-controlled inverters operate under the



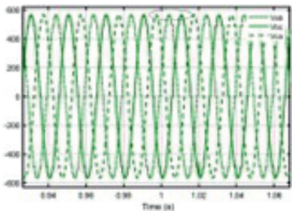
(a) Power status of SEMS



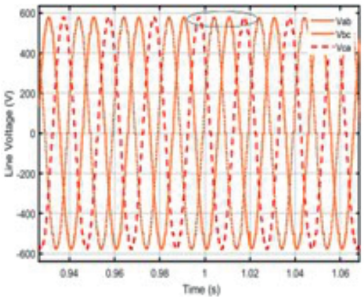
(b) Relay status of SEMS



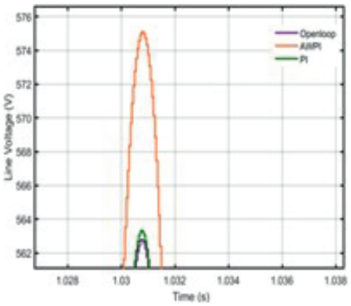
(c) Open loop inverter voltage



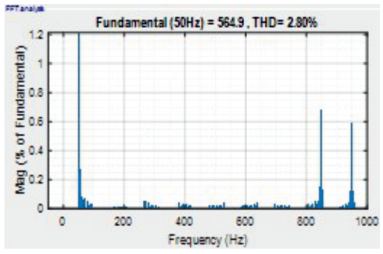
(d) PI controller inverter voltage



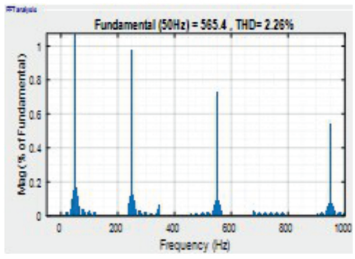
(e) AWPI controller inverter voltage



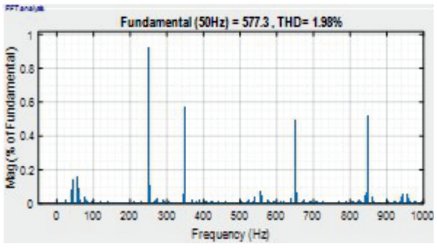
(f) Comparative analysis



(g) Voltage ThD – open loop



(h) Voltage ThD – PI



(i) Voltage ThD – AWPI

Fig. 3. Simulation results

same conditions. Figure 3(d) proves that the voltage drops by about 4 V when an inverter is integrated into the grid with PI control. Figure 3(e) shows that the voltage drops by about 1 V when an inverter is integrated into the grid. Figure 3(f) shows that, in contrast to PI and open-loop inverters, AWPI controllers enable the achievement of the maximum voltage. Figure 3(g) reveals an open-loop inverter with a PWM controller that achieves THD of 2.6%, which is within IEEE standards. Figure 3(h) shows that PI reduces THD to 2.26% when used in closed-loop voltage control of PWM. Figure 3(i) demonstrates how the lowered THD of 1.98%, which is less than the other two techniques, effectively controls AWPI.

Comparative performance of controller methods is shown in Table 1, which shows the details of various parameters before, during, and after grid integration.

Table 1

Comparative performance of controller methods

States with grid integration	Parameters	Control methods		
		Open loop	PI	AWPI
Before	Voltage THD (%)	2.52	2.25	1.97
	Current THD (%)	2.23	2.14	1.61
	Steady state error in voltage (%)	0.5172	0.4310	0.2241
During	Voltage drop (V)	4.5	4	1
After	Steady state error in voltage (%)	1.2069	1.1207	0.3966
	Voltage THD (%)	2.6	2.26	1.98
	Current THD (%)	2.24	2.16	1.63

Conclusion. An eminent energy management system with hybrid grid-tied inverter has been analyzed. The effectiveness of SEMS is examined under a variety of weather circumstances, battery SOC conditions, and load conditions, which confirms the SEMS's ability to meet its goals. During grid integration, control of grid-tied inverters employing various control approaches, such as AWPI controlled, PI controlled, and open loop, were analyzed through voltage and THD. The steady state error offered by PI is less than 1% before grid integration and above 1% after grid integration. Effective AWPI controlled inverter results in less than 0.5% under both states of grid integration. The variation in voltage with an AWPI-controlled, PI-controlled, and open-loop inverter during grid integration is 1 V, 4 V, and 4.5 V, respectively. These results infer the effectiveness of AWPI controller towards voltage regulation. Open-loop, PI-controlled, and AWPI-controlled inverters' respective THDs for voltage are 2.6%, 2.26%, and 1.98%, while THDs for current are 2.24%, 2.16% and 1.63%, respectively. AWPI's THD is lower than that of the other two approaches. In terms of voltage regulation and THD, AWPI performs better than PI and open loop inverters.

REFERENCES

[1] Ristic V., D. Sosic (2022) Novel DE-based optimization technique for the renewable sources' integration, C. R. Acad. Bulg. Sci., **75**(11), 1663–1671.

[2] Tenekeci M. E. (2023) Crack detection in photovoltaic panel electroluminescence image using matched filter for performance loss estimation, C. R. Acad. Bulg. Sci., **76**(2), 282–291.

[3] Li S., T. Zhang, X. Liu, Z. Xue, X. Liu (2022) Performance investigation of a grid-connected system integrated photovoltaic, battery storage and electric vehicles: A case study for gymnasium building, Energy and Buildings, **270**, 112255.

[4] Sharma S., Y. R. Sood, N. K. Sharma, M. Bajaj, H. M. Zawbaa et al. (2022) Modeling and sensitivity analysis of grid-connected hybrid green microgrid system, Ain Shams Eng. J., **13**(4), 101679.

[5] Jagadale P., A. Choudhari, S. Jadhav (2021) Design and simulation of grid connected solar Si-poly photovoltaic plant using PVsyst for Pune, India location, Renew. Energ. Res. Appl., **3**(1), 41–49.

[6] Kumar D. (2023) Overview to renewable energy systems. In: Renewable Energy Scenarios in Future Indian Smart Cities: A Geospatial Technology Perspective, Singapore, Springer Nature Singapore, 21–35.

[7] Farivar G. G., W. Manalastas, H. D. Tafti, S. Ceballos, A. Sanchez-Ruiz et al. (2022) Grid-connected energy storage systems: state-of-the-art and emerging technologies, Proc. IEEE, **111**(4), 397–420.

[8] Barakat S., A. Emam, M. M. Samy (2022) Investigating grid-connected green power systems energy storage solutions in the event of frequent blackouts, Energy Rep., **8**, 5177–5191.

[9] Yicheng Z., S. Jinhua, R. Yokoyama, Y. Nakanishi (2022) Implementation of P&O MPPT control for standalone PV system and its efficiency analysis. In: 2022 Int. Workshop on Intelligent Systems (IWIS), Ulsan, Republic of Korea, 1–4, https://doi.org/10.1109/IWIS56333.2022.9920779.

[10] Kumar S., C. Sethuraman (2022) Grid tied inverters for renewable energy systems – a review, Int. J. Environ. Sustain. Dev., **21**(1–2), 43–75.

[11] Bierhoff M., R. Soliman (2020) Analysis and design of grid-tied inverter with LCL filter, IEEE Open J. Power Electron., **1**, 161–169.

[12] Athari H., M. Niroomand, M. Ataei (2017) Review and classification of control systems in grid-tied inverters, Renew. Sust. Energ. Rev., **72**, 1167–1176.

[13] Lettl J., J. Bauer, L. Linhart (2011) Comparison of different filter types for grid-connected inverter, PIERS Proc., Marrakesh, Morocco, 20–23.

[14] Blaabjerg F., R. Teodorescu, M. Liserre, A. V. Timbus (2006) Overview of control and grid synchronization for distributed power generation systems, IEEE Trans. Ind. Electron., **53**(5), 1398–1409.

[15] Eren S., M. Pahlevani, A. Bakhshai, P. Jain (2015) An adaptive droop DC-bus voltage controller for a grid-connected voltage source inverter with LCL filter, IEEE Trans. Power Electron., **30**(2), 547–560.

[16] Bhattar C. L., M. A. Chaudhari (2023) Centralized energy management scheme for grid connected DC microgrid, IEEE Syst. J., 1–11.

[17] Aloo L. A., P. K. Kihato, S. I. Kamau, R. S. Orenge (2023) Modeling and control of a photovoltaic-wind hybrid microgrid system using GA-ANFIS, Heliyon, **9**(4), e14678.

[18] Sivakumar S., M. J. Sathik, P. S. Manoj, G. Sundararajan (2016) An assessment on performance of DC-DC converters for renewable energy applications, Renew. Sust. Energ. Rev., **58**, 1475–1485.
[19] Choi J. W., S. C. Lee (2009) Antiwindup strategy for PI-type speed controller, IEEE Trans. Ind. Electron., **56**(6), 2039–2046.
[20] Eldigair Y., F. Garelli, C. Kunusch, C. Ocampo-Martinez (2020) Adaptive PI control with robust variable structure anti-windup strategy for systems with rate-limited actuators: Application to compression systems, Control. Eng. Pract., **96**, 104282.

Department of Electrical
and Electronics Engineering
Sri Eshwar College of Engineering
Coimbatore 641 202, Tamilnadu, India
e-mail: sheikameerbatcha.s1@gmail.com

Department of Electronics
and Communication Engineering
Sri Eshwar College of Engineering
Coimbatore 641 202, Tamilnadu, India
e-mail: principal@sece.ac.in